On-chip microwave photonic beamformer circuits operating with phase modulation and direct detection

Leimeng Zhuang,[1,2,3,7,*] Marcel Hoekman,[4] Caterina Taddei,[1,6] Arne Leinse,[4] René G. Heideman,[4] Adriaan Hulzinga,[2] Jaco Verpoorte,[2] Ruud M. Oldenbeuving,[5] Paulus W. L. van Dijk,[5] Klaus-J. Boller,[6] and Chris G. H. Roeloffzen[1,5]

[1]*Telecommunication Engineering group, University of Twente, PO Box 217, Enschede, 7500 AE, The Netherlands*
[2]*National Aerospace Laboratory (NLR), PO Box 153, Emmeloord, 8300 AD, The Netherlands*
[3]*Current: Monash Electro-Photonics Laboratory, Dept. of Electrical and Computer Systems Engineering, Monash University, Clayton, VIC 3800, Australia*
[4]*LioniX BV, PO Box 456, Enschede, 7500 AL, The Netherlands*
[5]*SATRAX BV, PO Box 456, Enschede, 7500 AL, The Netherlands*
[6]*Laser Physics and Nonlinear Optics group, PO Box 217, Enschede, 7500 AL, The Netherlands*
[7]*l.zhuang@utwente.nl*
**leimeng.zhuang@monash.edu*

Abstract: We propose and experimentally demonstrate the working principles of two novel microwave photonic (MWP) beamformer circuits operating with phase modulation (PM) and direct detection (DD). The proposed circuits incorporate two major signal processing functionalities, namely a broadband beamforming network employing ring resonator-based delay lines and an optical sideband manipulator that renders the circuit outputs equivalent to those of intensity-modulated MWP beamformers. These functionalities allow the system to employ low-circuit-complexity modulators and detectors, which brings significant benefits on the system construction cost and operation stability. The functionalities of the proposed MWP beamformer circuits were verified in experimental demonstrations performed on two sample circuits realized in Si_3N_4/SiO_2 waveguide technology. The measurements exhibit a 2 × 1 beamforming effect for an instantaneous RF transmission band of 3–7 GHz, which is, to our best knowledge, the first verification of on-chip MWP beamformer circuits operating with PM and DD.

OCIS codes: (130.3120) Integrated optics devices; (060.5625) Radio frequency photonics; (070.6020) Continuous optical signal processing; (060.2360) Fiber optics links and subsystems; (350.4010) Microwaves.

References and links

1. D. Dolfi, F. Michel-Gabriel, S. Bann, and J. P. Huignard, "Two-dimensional optical architecture for time-delay beam forming in a phased-array antenna," Opt. Lett. **16**(4), 255–257 (1991).
2. N. A. Riza, "Liquid crystal-based optical control of phased array antennas," J. Lightwave Technol. **10**(12), 1974–1984 (1992).
3. N. A. Riza, "Acousto-optic liquid-crystal analog beam former for phased-array antennas," Appl. Opt. **33**(17), 3712–3724 (1994).
4. W. Ng, A. A. Walston, G. L. Tangonan, J. J. Lee, I. L. Newberg, and N. Bernstein, "The first demonstration of an optically steered microwave phased array antenna using true-time-delay," J. Lightwave Technol. **9**(9), 1124–1131 (1991).
5. J. L. Corral, J. Mart, S. Regidor, J. M. Foster, R. Laming, and M. J. Cole, "Continuously variable true time-delay optical feeder for phased-array antenna employing chirped fiber gratings," IEEE Trans. Microw. Theory Tech. **45**(8), 1531–1536 (1997).
6. N. A. Riza, "Analog vector modulation-based widely tunable frequency photonic beamformer for phased array antennas," IEEE Trans. Microw. Theory Tech. **45**(8), 1508–1512 (1997).
7. L. A. Bui, A. Mitchell, K. Ghorbani, T. Chio, S. Mansoori, and E. R. Lopez, "Wide-band photonically phased array antenna using vector sum phase shifting approach," IEEE Trans. Antenn. Propag. **53**(11), 3589–3596 (2005).

#211835 - $15.00 USD Received 9 May 2014; revised 26 Jun 2014; accepted 27 Jun 2014; published 3 Jul 2014

8. J. Stulemeijer, F. E. van Vliet, K. W. Benoist, D. H. P. Maat, and M. K. Smit, "Compact photonic integrated phase and amplitude controller for phased-array antennas," IEEE Photon. Technol. Lett. **11**(1), 122–124 (1999).
9. F. M. Soares, F. Karouta, E. Smalbrugge, M. K. Smit, J. j. M. Binsma, J. Lopez, A. Enard, and V. Vodjdani, "An InP-based photonic integrated beamformer for phased-array antennas," Proc. Optical Amplifiers and Their Applications/Integrated Photonics Research, Technical Digest, paper IFB2 (2004).
10. L. Zhuang, C. G. H. Roeloffzen, R. G. Heideman, A. Borreman, A. Meijerink, and W. C. van Etten, "Single-chip ring resonator-based 1 × 8 optical beamforming network in CMOS-compatible waveguide technology," IEEE Photon. Technol. Lett. **19**(15), 1130–1132 (2007).
11. A. Meijerink, C. G. H. Roeloffzen, R. Meijerink, L. Zhuang, D. A. I. Marpaung, M. J. Bentum, M. Burla, J. Verpoorte, P. Jorna, A. Hulzinga, and W. C. van Etten, "Novel ring resonator-based integrated photonic beamformer for broadband phased array receive antennas–part I: design and performance analysis," J. Lightwave Technol. **28**(1), 3–18 (2010).
12. L. Zhuang, C. G. H. Roeloffzen, A. Meijerink, M. Burla, D. A. I. Marpaung, A. Leinse, M. Hoekman, R. G. Heideman, and W. C. van Etten, "Novel ring resonator-based integrated photonic beamformer for broadband phased-array antennas-Part II: experimental prototype," J. Lightwave Technol. **28**(1), 19–31 (2010).
13. J. D. Doménech, P. Muñoz, and J. Capmany, "Discretely tunable microwave photonics beamformer based on ring resonators and arrayed waveguide gratings," Proc. SPIE7719 (2010).
14. M. Burla, C. G. H. Roeloffzen, L. Zhuang, D. A. I. Marpaung, M. R. Khan, P. Maat, K. Dijkstra, A. Leinse, M. Hoekman, and R. Heideman, "System integration and radiation pattern measurements of a phased array antenna employing an integrated photonic beamformer for radio astronomy applications," Appl. Opt. **51**(7), 789–802 (2012).
15. F. Xiao, B. Juswardy, K. Alameh, S. Xiao, and W. Hu, "Opto-VLSI-Based Beamformer for radio-frequency phased-array antennas," IEEE Photon. J. **4**(3), 912–919 (2012).
16. M. Burla, D. A. I. Marpaung, L. Zhuang, M. Hoekman, R. G. Heideman, and C. G. H. Roeloffzen, "Integrated photonic K_u-band Beamformer chip with continuous Amplitude and Delay Control," IEEE Photon. Technol. Lett. **25**(12), 1145–1148 (2013).
17. M. Burla, D. Marpaung, L. Zhuang, M. R. Khan, A. Leinse, W. P. Beeker, M. Hoekman, R. G. Heideman, and C. G. H. Roeloffzen, "Multi-wavelength integrated optical beamformer based on wavelength division multiplexing and separate carrier tuning," J. Lightwave Technol. (to be published).
18. X. K. Yi, T. X. Huang, and R. A. Minasian, "Photonic beamforming based on programmable phase shifters with amplitude and phase control," IEEE Photon. Technol. Lett. **23**(18), 1286–1288 (2011).
19. Y. Zhang, H. Wu, D. Zhu, and S. Pan, "An optically controlled phased array antenna based on single sideband polarization modulation," Opt. Express **22**(4), 3761–3765 (2014).
20. S. Plass, ed., *Future aeronautical communications* (InTech, 2011), Chap. 10.
21. J. Capmany and D. Novak, "Microwave photonics combines two worlds," Nat. Photonics **1**(6), 319–330 (2007).
22. J. Yao, "Microwave photonics," J. Lightwave Technol. **27**(3), 314–335 (2009).
23. C. G. H. Roeloffzen, L. Zhuang, C. Taddei, A. Leinse, R. G. Heideman, P. W. L. van Dijk, R. M. Oldenbeuving, D. A. I. Marpaung, M. Burla, and K.-J. Boller, "Silicon nitride microwave photonic circuits," Opt. Express **21**(19), 22937–22961 (2013).
24. D. A. I. Marpaung, C. G. H. Roeloffzen, R. G. Heideman, A. Leinse, S. Sales, and J. Capmany, "Integrated microwave photonics," Laser Photonics Rev. **7**(4), 506–538 (2013).
25. N. N. Feng, P. Dong, D. Feng, W. Qian, H. Liang, D. C. Lee, J. B. Luff, A. Agarwal, T. Banwell, R. Menendez, P. Toliver, T. K. Woodward, and M. Asghari, "Thermally-efficient reconfigurable narrowband RF-photonic filter," Opt. Express **18**(24), 24648–24653 (2010).
26. B. Guan, S. S. Djordjevic, N. K. Fontaine, L. Zhou, S. Ibrahim, R. P. Scott, D. J. Geisler, Z. Ding, and S. J. B. Yoo, "CMOS compatible reconfigurable silicon photonic lattice filters using cascaded unit cells for RF-photonic processing," IEEE J. Sel. Top. Quantum Electron. **20**(14), 8202110 (2014).
27. R. S. Guzzon, E. J. Norberg, J. S. Parker, L. A. Johansson, and L. A. Coldren, "Integrated InP-InGaAsP tunable coupled ring optical bandpass filters with zero insertion loss," Opt. Express **19**(8), 7816–7826 (2011).
28. M. H. Khan, H. Shen, Y. Xuan, L. Zhao, S. Xiao, D. E. Leaird, A. M. Weiner, and M. Qi, "Ultrabroad-bandwidth arbitrary radiofrequency waveform generation with a silicon photonic chip-based spectral shaper," Nat. Photonics **4**(2), 117–122 (2010).
29. F. M. Soares, N. K. Fontaine, R. P. Scott, J. H. Baek, X. Zhou, T. Su, S. Cheung, Y. Wang, C. Junesand, S. Lourdudoss, K. Y. Liou, R. A. Hamm, W. Wang, B. Patel, L. A. Gruezke, W. T. Tsang, J. P. Heritage, and S. J. B. Yoo, "Monolithically integrated InP 100-channel X 10-GHz device for optical arbitrary waveform generation," IEEE Photon. J. **3**(6), 975–985 (2011).
30. M. Ferrera, Y. Park, L. Razzari, B. E. Little, S. T. Chu, R. Morandotti, D. J. Moss, and J. Azaña, "On-chip CMOS-compatible all-optical integrator," Nat Commun **1**(3), 29 (2010), doi:10.1038/ncomms1028.
31. W. Liu, M. Li, R. S. Guzzon, E. J. Norberg, J. S. Parker, L. A. Coldren, and J. Yao, "A photonic temporal integrator with an ultra-long integration time window based on an InP-InGaAsP integrated ring resonator," J. Lightwave Technol. **99**, 1 (2014).
32. F. Liu, T. Wang, L. Qiang, T. Ye, Z. Zhang, M. Qiu, and Y. Su, "Compact optical temporal differentiator based on silicon microring resonator," Opt. Express **16**(20), 15880–15886 (2008).
33. J. Dong, A. Zheng, D. Gao, L. Lei, D. Huang, and X. Zhang, "Compact, flexible and versatile photonic differentiator using silicon Mach-Zehnder interferometers," Opt. Express **21**(6), 7014–7024 (2013).
34. J. S. Fandiño, J. D. Doménech, P. Muñoz, and J. Capmany, "Integrated InP frequency discriminator for Phase-modulated microwave photonic links," Opt. Express **21**(3), 3726–3736 (2013).

#211835 - $15.00 USD Received 9 May 2014; revised 26 Jun 2014; accepted 27 Jun 2014; published 3 Jul 2014

35. D. A. I. Marpaung, C. G. H. Roeloffzen, A. Leinse, and M. Hoekman, "A photonic chip based frequency discriminator for a high performance microwave photonic link," Opt. Express **18**(26), 27359–27370 (2010).
36. W. Xue, S. Sales, J. Capmany, and J. Mørk, "Wideband 360 ° microwave photonic phase shifter based on slow light in semiconductor optical amplifiers," Opt. Express **18**(6), 6156–6163 (2010).
37. J. Lloret, G. Morthier, F. Ramos, S. Sales, D. Van Thourhout, T. Spuesens, N. Olivier, J. M. Fédéli, and J. Capmany, "Broadband microwave photonic fully tunable filter using a single heterogeneously integrated III-V/SOI-microdisk-based phase shifter," Opt. Express **20**(10), 10796–10806 (2012).
38. J. Lloret, G. Morthier, F. Ramos, S. Sales, D. Van Thourhout, T. Spuesens, N. Olivier, J. M. Fédéli, and J. Capmany, "Broadband microwave photonic fully tunable filter using a single heterogeneously integrated III-V/SOI-microdisk-based phase shifter," Opt. Express **20**(10), 10796–10806 (2012).
39. J. Capmany, D. Doménech, and P. Muñoz, "Silicon graphene waveguide tunable broadband microwave photonics phase shifter," Opt. Express **22**(7), 8094–8100 (2014).
40. M. Burla, D. A. I. Marpaung, L. Zhuang, C. G. H. Roeloffzen, M. R. Khan, A. Leinse, M. Hoekman, and R. G. Heideman, "On-chip CMOS compatible reconfigurable optical delay line with separate carrier tuning for microwave photonic signal processing," Opt. Express **19**(22), 21475–21484 (2011).
41. L. Zhuang, M. Hoekman, A. Leinse, R. G. Heideman, P. W. L. van Dijk, and C. G. H. Roeloffzen, "Novel low-loss waveguide delay line using Vernier ring resonators for on-chip multi-λ microwave photonic signal processors," Laser Photon. Rev. **7**(6), 994–1002 (2013).
42. J. Sancho, J. Bourderionnet, J. Lloret, S. Combrié, I. Gasulla, S. Xavier, S. Sales, P. Colman, G. Lehoucq, D. Dolfi, J. Capmany, and A. De Rossi, "Integrable microwave filter based on a photonic crystal delay line," Nat Commun **3**, 1075 (2012).
43. R. Pant, D. Marpaung, I. V. Kabakova, B. Morrison, C. G. Poulton, and B. J. Eggleton, "On-chip stimulated Brillouin scattering for microwave signal processing and generation," Laser Photon. Rev. (2014).
44. L. Zhuang, D. A. I. Marpaung, M. Burla, W. P. Beeker, A. Leinse, and C. G. H. Roeloffzen, "Low-loss, high-index-contrast Si_3N_4/SiO_2 optical waveguides for optical delay lines in microwave photonics signal processing," Opt. Express **19**(23), 23162–23170 (2011).
45. L. Zhuang, M. R. Khan, W. P. Beeker, A. Leinse, R. G. Heideman, and C. G. H. Roeloffzen, "Novel microwave photonic fractional Hilbert transformer using a ring resonator-based optical all-pass filter," Opt. Express **20**(24), 26499–26510 (2012).
46. L. Zhuang, C. Taddei, M. Hoekman, A. Leinse, R. G. Heideman, P. W. L. van Dijk, and C. G. H. Roeloffzen, "Ring resonator-based on-chip modulation transformer for high-performance phase-modulated microwave photonic links," Opt. Express **21**(22), 25999–26013 (2013).
47. J. S. Fandino, M. Rius, J. Mora, P. Munoz, and J. Capmany, "Optical Single Sideband Transmitter using Phase Modulation and a Photonic Integrated Filter," 2013 IEEE International Topical Meeting on Microwave Photonics (MWP2013), 28–31 Oct., Alexandra, VA, USA.
48. L. Zhuang, W. P. Beeker, A. Leinse, R. G. Heideman, P. van Dijk, and C. Roeloffzen, "Novel wideband microwave polarization network using a fully-reconfigurable photonic waveguide interleaver with a two-ring resonator-assisted asymmetric Mach-Zehnder structure," Opt. Express **21**(3), 3114–3124 (2013).
49. L. Zhuang, M. Hoekman, R. M. Oldenbeuving, K.-J. Boller, and C. G. H. Roeloffzen, "CRIT-alternative narrow-passband waveguide filter for microwave photonic signal processors," IEEE Photon. Technol. Lett. **26**(10), 1034–1037 (2014).
50. R. J. Mailoux, *Phased Array Antenna Handbook* (Artech House, 2005).
51. C. K. Madsen and J. H. Zhao, *Optical Filter Design and Analysis* (Wiley, 1999).

1. Introduction

Microwave photonic (MWP) beamformers for RF phased array antennas have stimulated a fast-growing surge of interest in the past decades from both scientific and industrial communities [1–19]. In particular, promising applications for airborne and spaceborne communications and large-scale-antenna-based radio astronomy have shown the added value of and need for microwave photonic technologies [20]. By harnessing the advantageous nature of photonics, MWP beamformers allow the pursued system features such as large instantaneous RF bandwidth, light weight, low loss, high system compactness, beam pattern reconfigurability, and seamless beam-steering to be achieved simultaneously [21, 22]. Nevertheless, it is believed that MWP beamformers, just like the other promising MWP functionalities, can only become a widely-deployed and commercially competitive solution as against the conventional all-electronics ones when the full integration of the MWP systems has been successfully achieved [23, 24]. The integrated method is known to be most effective way to bring down the system costs to a level allowing for volume production. A more fundamental aspect is that it improves system stability and predictability, which is essential for the success in meeting the ever-rising performance requirements. In the context of MWP beamformer, integrating the photonic functionalities in the chip level will not only enable precise light manipulation at the wavelength scale, but also make it possible to create very

#211835 - $15.00 USD Received 9 May 2014; revised 26 Jun 2014; accepted 27 Jun 2014; published 3 Jul 2014

complex systems for large-scale phased array antennas, where a great number of devices and dense control are required [20]. Next to the beamformer [8-17], a significant number of other key MWP functionalities have also been demonstrated in the recent years using different integration technologies [24]. Some salient works include reconfigurable filters [25-27], arbitrary waveform generators [28, 29], integrators [30, 31], differentiators [32, 33], frequency discriminators [34, 35], and tunable phase shifters and delay lines [36–43].

In our previous works, we have proposed and demonstrated a number of integrated beamformer circuits, which are realized in low-loss, high-index-constrast Si_3N_4/SiO_2 planar waveguides (TriPleX waveguide technology) [10, 12, 14, 16, 17, 20, 23, 44]. These on-chip beamformer circuits implement a number of key-functionalities such as broadband beamforming networks employing ring resonator-based delay lines [10, 41], optical sideband filters [14, 23, 44], separate carrier phase tuning [40], and (de)multiplexers operating in both RF and optical regimes [17]. All these functionalities are designed to be continuously tunable by incorporating thermo-optical tuning elements in the circuits. This enables the proposed beamformers to perform arbitrary beamforming and seamless beam-steering, which are difficult to achieve using the conventional all-electronics beamformers. In addition to this, more advanced functionalities such as multi-beam and multi-RF band beamforming are also possible to be implemented in the beamformer circuits by exploiting signal processing schemes based on the frequency periodicity of the waveguide devices and simultaneous use of multiple optical wavelengths [16, 17].

For the previously demonstrated MWP beamformers, the antenna signals are typically up-converted into the optical domain by means of optical intensity modulation using Mach-Zehnder modulators or electroabsorption modulators. In general, intensity modulators require, in practice, bias-voltage adjustment and stabilization for optimum performance. Besides, their implementations usually involve a trade-off between device performance and complexity. All this may lead to critical risks for the realization of fully integrated MWP beamformers, particularly when an array of multiple modulators is required in receive antennas. In contrast, phase modulators feature not only high modulation efficiency and bias-free operation, but also low device complexity thereby reducing risks in device realization. Calling upon this fact and the aim of low system complexity, it is therefore worth investigating the implementation of MWP beamformers operating with phase modulation (PM) and direct detection (DD).

Here we propose and experimentally verify two on-chip MWP beamformer circuits which allow for such PM/DD scheme. The circuits incorporate two major signal processing functionalities: one is a 2 × 1 beamforming network employing ring resonator-based delay lines which enables seamless beam-steering for broadband antennas; the other is an optical sideband manipulator (OSM) which renders the circuit output equivalent to those of intensity modulation. The implementation of the OSM functionality enables the use of simple direct detection in the system instead of high-device-complexity coherent detection. In Section 2, the working principles of the MWP beamformers operating with PM and DD are explained. Section 3 describes the architectures of the beamformer circuits and the parameter settings for operation. In Section 4, the experimental demonstrations of the circuit functionalities are presented. The conclusions and discussions are given in Section 5.

2. System principle

The proposed MWP beamformer system incorporating the PM/DD scheme is schematically depicted in Fig. 1. The signal processing schemes applied are conceptually illustrated in Fig. 2, where the amplitude and phase spectra of the signals are shown at different points throughout the scheme to illustrate the working of the system. As depicted in Fig. 1, beamforming is considered using the simplified model of a two-element phased array receive antenna. Here, we use the far-field plane-wave assumption for the incident RF signal. In this example, the signal incident angle with respect to the normal of the antenna plane is indicated by θ, with which the lower antenna element receives a wavefront of the incident RF signal with a time delay $\Delta\tau$ (determined by $\Delta\tau = \sin(\theta)d/c_0$ with d the inter-element distance and c_0 the speed of light in air) as against the upper one as shown in Fig. 1. We use $s(t)$ and $s(t-\Delta\tau)$

#211835 - $15.00 USD Received 9 May 2014; revised 26 Jun 2014; accepted 27 Jun 2014; published 3 Jul 2014

to represent the upper and lower antenna element output respectively, which drive two phase modulators for electrical-to-optical conversion. The modulators are optically fed by a CW, single-frequency laser source via a power splitter. In the optical domain, the modulated optical signals at point A and B show up with different phase characteristics as illustrated by $\phi_A(f)$ and $\phi_B(f)$ in Fig. 2. Here, point A is regarded as the signal reference. For simplicity, the phase modulation is described by a flat phase characteristic and an overall phase shift of $\pi/2$ with respect to the optical carrier. Relative to this reference, the signal at point B shows a linear phase characteristic resulting from the antenna delay $\Delta\tau$, with which the phase slope scales. To achieve the beamforming functionality [11, 14, 50], the optical signals at point C and D are required to be synchronized in both phase and delay, so that at point E they will add up constructively for the entire signal band. To this end, a tunable optical time delay line (TTD) and an optical phase shifter (OPS) are used in the beamformer circuit as shown in Fig. 1. Assuming that both the TTD and OPS have optical bandwidths to cover the entire modulation spectrum, then the optical signals at point C and D can be made identical when the TTD provides a delay equal to $\Delta\tau$ and OPS removes the carrier phase difference between the two signal paths. Next to the question on the phase, the relative amplitudes between different signal paths are also a determining factor for the beamforming functionality [11, 14, 50]. In practice, this can be addressed by implementing the signal combiner (between point C/D and E in Fig. 1) using an arbitrary-ratio tunable coupler [23, 44], which also compensates the loss difference between the signal paths.

Although constructively combined as shown in the inset E of Fig. 2, the optical signal at point E is still in the phase modulation format. This means that the desired RF signal cannot yet be recovered by means of direct detection at that point, because the two phase modulation sidebands will contribute to the RF output in anti-phase status and therefore cancel out each other. To render the output of the beamformer circuit detectable by means of direct detection, or in other words, equivalent to that of intensity modulation, a dedicated processing unit is added in serial to the signal synchronizing and combining functionalities, namely a so-called optical sideband manipulator (OSM). Basically, this OSM can perform its function via two alternative approaches as illustrated in the inset F-case 1 and F-case 2 of Fig. 2. In F-case 1, the approach is to provide an additional phase shift of π, as indicated by $\Delta\phi_{OSM}(f)$, to one of the sidebands (the upper sideband is subject to this phase shift in the illustration; besides, the general slope $\Delta\tau'$ indicates an extra delay introduced by the device). As a result of this, the two sidebands feature anti-symmetrical phases with respect to the optical carrier, which is then equivalent to the spectrum characteristic of intensity modulation [45, 46]. The other approach is to remove one of the sidebands from the optical signal by using a spectral filter with a transfer function $\Delta|H_{OSM}(f)|$ as shown in F-case 2 [47-49]. This way, only the remaining sideband contributes to the RF output, which prevents the RF cancellation effect and therefore makes direct detection viable. However, unlike that for the first approach, the detected RF output in this case has an additional loss of 3 dB because half of the signal power is lost by filtering. On the other hand, this filter approach has a benefit of a significantly lower optical bandwidth requirement for the TTD, since the TTD only needs to have a delay bandwidth to cover one sideband and the optical carrier rather than the entire modulation spectrum. As will be explained later, this may lead to lower device complexity when ring resonators are used to construct the TTD.

In principle, the order of the aforementioned processing functionalities can be inverted. This means that the proposed beamformer circuit can also be applied to transmit antennas when the modulators are replaced by the detectors and vice versa. Although so far we considered only the simplest scenario of beamforming with two antenna elements, the concept of such a beamformer with the PM/DD scheme also applies to large-scale phased array antennas consisting of N ($N > 2$) antenna elements. For example, an $N \times 1$ combining circuitry can be constructed using multiple 2×1 combiners arranged in a binary-tree topology. The TTD and OPS functionalities can be equipped to every signal path to facilitate a flexible beamformer which supports arbitrary beamforming for 2-D phased array antennas [14, 17, 20]. However, from the perspective of device realization and operation, upscaling the

#211835 - $15.00 USD Received 9 May 2014; revised 26 Jun 2014; accepted 27 Jun 2014; published 3 Jul 2014

beamformer also raises a number of challenges. Larger antenna dimensions means longer delays required on chip, which cause higher device insertion loss because the optical transmission loss scales with the effective delay path length. This accents more the need of a low-loss integration platform. For the receive antennas, the on-chip realization of an array of high-transfer-efficiency modulators is seen to be essential for the system operation, not only because of the questions on the performance and cost, but more fundamentally the integration of this with the beamformer circuit preserves the inter-channel phase relation which enables coherent optical processing as required in the system principle. Although not yet mature, some significant progress for this has been made in the development of monolithic or hybrid photonic integration technologies [20]. Moreover, as the beamformer becomes more complex with more functional units incorporated, the dynamic control of it becomes also a concern. This requires then devising a dedicated algorithm, which can be implemented either by means of real-time computing or switching between different settings of a look-up table, depending on the applications.

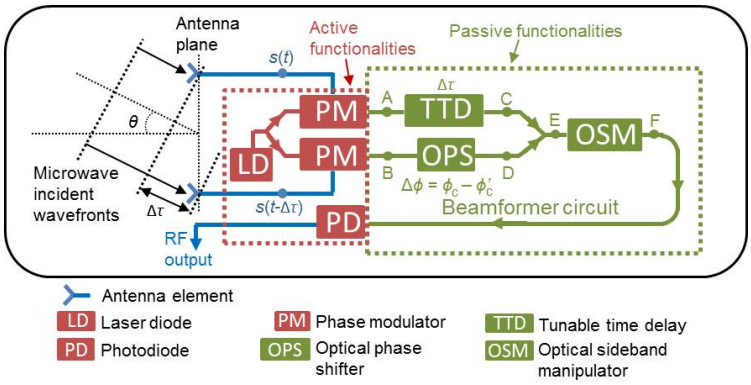

Fig. 1. A schematic of the MWP beamformer system associating the PM/DD scheme for a 2-element phased array receive antenna. The devices indicated in the filled blocks are envisioned to be integrated in the chip level using a monolithic or hybrid integration platform.

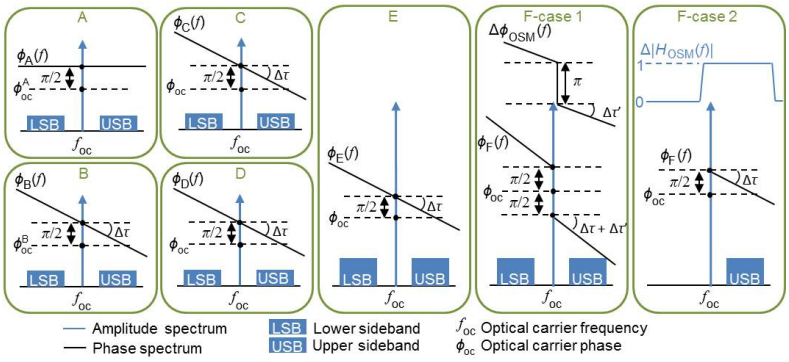

Fig. 2. Conceptual illustrations of the signal amplitude and phase spectra at different position points in the system shown in Fig. 1 (A: the optical signal spectrum is considered to be the reference, having a flat phase characteristic for simplicity; B: the optical signal spectrum including a linear phase characteristic caused by the antenna delay Δτ; C and D: the optical signals in both beamformer channels are synchronized in delay as well as optical carrier phase, by means of the tunable delay line (TTD) and optical phase shifter (OPS) as indicated in Fig. 1; E: two beamformer channels are combined constructively; F-case 1: phase-modulation to intensity-modulation (PM-to-IM) conversion by means of a ring resonator-based modulation transformer (MT), which introduces an additional phase shift of π to one of the sidebands (the upper sideband in this illustration) so that the signal spectrum is an equivalent to that of intensity modulation; F-case 2: PM-to-IM conversion based on an optical sideband filter (OSBF), which removes one of the sidebands and makes direct detection viable).

#211835 - $15.00 USD Received 9 May 2014; revised 26 Jun 2014; accepted 27 Jun 2014; published 3 Jul 2014

3. Beamformer circuits

To implement the processing functionalities of the beamformer described above, we consider two architectures of waveguide circuits, which are depicted in Fig. 3(a) and 3(b). The circuits are constructed using only three basic building blocks, which are tunable couplers (in this case 2 × 2 Mach-Zehnder couplers), ring resonators, and phase shifters. The tunable coupler can be used in the circuits as a signal combiner/splitter or switch, where the coupling coefficient κ can be varied by changing the optical phase shift difference between the two arms [23, 44]. A practical way to achieve an additional optical phase shift ϕ is to modify the refractive index over a length of waveguide, such as via incorporating a thermo-optical or electro-optical tuning element. As depicted in Fig. 3(c), a fully-tunable ring resonator can be constructed by incorporating one arm of the Mach-Zehnder coupler in a closed loop and adding two such tuning elements to obtain tunability of κ and ϕ. This tunability allows us to compensate for the fabrication tolerance and achieve arbitrary delay settings as the delay value (which is proportional to the quality factor [51]) and the resonance frequency of the ring resonator can be varied by changing κ and ϕ, respectively [12, 41, 44]. For the implementation of TTD and OPS functionalities, we chose here cascades of ring resonators and independent phase tuning elements, respectively. Our earlier works have demonstrated that they are able to perform desired functionalities for broadband signals and are particularly good candidates for constructing compact circuits [12, 14]. As the two options to realize an OSM as described above, circuit architecture 1 implements the phase-shift approach, using a single ring resonator serving as a phase-to-intensity modulation transformer (MT) [45, 46], and circuit architecture 2 implements the spectral-filtering approach, using an optical sideband filter (OSBF) based on a ring resonator-assisted Mach-Zehnder interferometer (RAMZI) structure [44, 47-49].

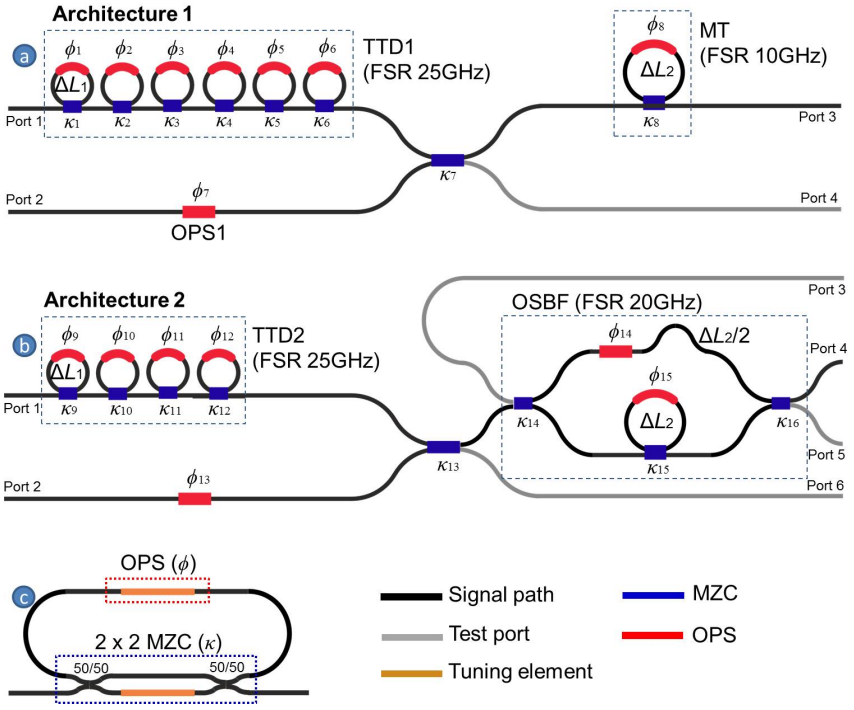

Fig. 3. (a) beamformer circuit architecture 1 including a ring resonator-based modulation transformer (MT); (b) beamformer circuit architecture 2 including an optical sideband filter (OSBF) based on ring resonator-assisted Mach-Zehnder interferometer structure; (c) the structure breakdown of a fully-tunable ring resonator.

#211835 - $15.00 USD Received 9 May 2014; revised 26 Jun 2014; accepted 27 Jun 2014; published 3 Jul 2014

To give a concrete example of circuit design, we consider here a 2 × 1 beamforming functionality for an RF signal specification: a center frequency of 5 GHz, an instantaneous bandwidth of 4 GHz (3–7 GHz), and a maximum delay difference of 0.3 ns between the two antenna elements. Based on the system principle shown in Fig. 1, the ideal frequency responses of the TTD and OSM for both circuit architectures can be defined accordingly, which are the dotted lines in Fig. 4. To prove of concept, we consider using the Si_3N_4/SiO_2 waveguide technology as described in [44] to construct the circuits. This allows the TTDs to be constructed using a cascade of ring resonators with a free spectral range (FSR) of 25 GHz, which features device compactness and low propagation loss (systematically ≤ 0.15 dB/cm) simultaneously. Based on the bandwidth properties investigated in [45-49], FSRs of 10 GHz and 20 GHz are chosen for the MT and OSBF, respectively, such that their operation passbands are sufficiently wide to accommodate the specified RF signal. In the context of signal processing, one can use z-transforms to describe the transfer functions of the waveguide circuits and calculate the corresponding frequency responses [51]. Then, by approximating the calculated frequency responses of the implemented TTDs and OSMs to the ideal ones, one can determine the needed number of cascaded ring resonators and the circuit parameters (κ and ϕ) to achieve the desired beamforming functionality. An example of the approximation is depicted in solid lines in Fig. 4, for which the z-transforms and circuit parameter setting for circuit architecture 1 and 2 are listed in Table 1. Here, the power transmission coefficient $r = 0.96$ is used for calculation, which corresponds to the low-loss Si_3N_4/SiO_2 waveguide (0.15 dB/cm) and has negligible effect on the circuit functionalities. The optical carrier frequency is regarded as the frequency reference for setting the circuit frequency responses. For circuit architecture 1, we calculate that 6 ring resonators are needed to allow the TTD to fulfill the delay bandwidth requirement, which is, in this case, a bandwidth ≥ 14 GHz to cover the entire spectrum of the optical signal including the carrier and both upper and lower sidebands. In coordination, the MT with a FSR of 10 GHz introduces a phase shift of π to the lower sideband with respect to the carrier and upper sideband. This implements the signal processing scheme "F-case 1" in Fig. 2. For circuit architecture 2, a smaller number of ring resonators, namely 4 ring resonators in this case, is sufficient for the TTD to satisfy the delay bandwidth requirement, since the lower sideband will be removed from the signal spectrum by filtering and the actual signal bandwidth reduces thereby to 7 GHz. The OSBF with a FSR of 20 GHz is characterized by a passband with a bandwidth of 10 GHz, a stopband 6 GHz, and a transition band 2 GHz. This matches the specification of the optical signal spectrum and implements the signal processing scheme "F-case 2" in Fig. 2.

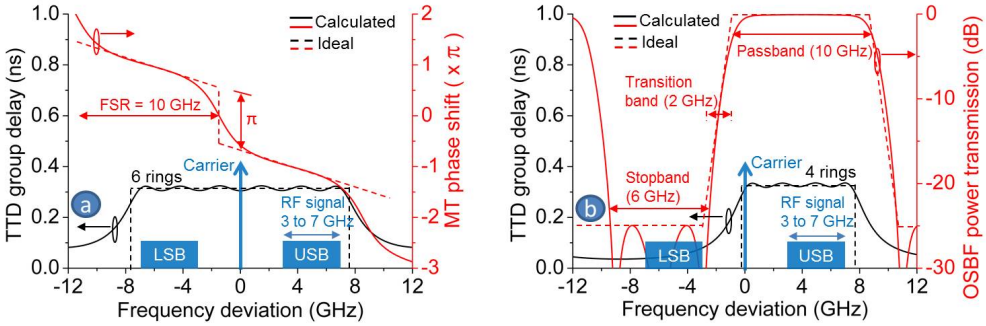

Fig. 4. The graphs in (a) and (b) depict the calculated true time delay (TTD) and optical sideband manipulator (OSM) responses (solid lines) of circuit 1 and 2, respectively, which are set to approximate the ideal responses (dotted lines) for the 2 × 1 beamforming functionality. The circuit parameter setting for the approximation is given in Table 1. The blue sketches indicate the relative spectral positions of the carrier and the upper and lower sidebands (USB, LSB) of the optical signals.

#211835 - $15.00 USD Received 9 May 2014; revised 26 Jun 2014; accepted 27 Jun 2014; published 3 Jul 2014

Table 1. List of *z*-transforms and parameter settings of the proposed beamformer circuits

	Architecture 1 (Fig. 3(a))	Architecture 2 (Fig. 3(b))
TTD	**6 ring resonators (FSR 25 GHz):**	**4 ring resonators (FSR 25 GHz):**
	$H_{\mathrm{TTD1}}(z)=\prod_{n=1}^{6}H_{\mathrm{RR},n}(z)$ $=\prod_{n=1}^{6}\frac{\sqrt{1-\kappa_n}-e^{-j\phi_n}z^{-1}\sqrt{r}}{1-e^{-j\phi_n}z^{-1}\sqrt{r(1-\kappa_n)}}$	$H_{\mathrm{TTD2}}(z)=\prod_{n=9}^{12}H_{\mathrm{RR},n}(z)$ $=\prod_{n=9}^{12}\frac{\sqrt{1-\kappa_n}-e^{-j\phi_n}z^{-1}\sqrt{r}}{1-e^{-j\phi_n}z^{-1}\sqrt{r(1-\kappa_n)}}$
	$\kappa_1 = 0.55$; $\kappa_2 = 0.62$; $\kappa_3 = 0.63$; $\kappa_4 = 0.63$; $\kappa_5 = 0.62$; $\kappa_6 = 0.55$; $\phi_1 = 0.56\pi$; $\phi_2 = 0.34\pi$; $\phi_3 = 0.12\pi$; $\phi_4 = -0.12\pi$; $\phi_5 = -0.34\pi$; $-\phi_6 = 0.56\pi$.	$\kappa_9 = 0.52$; $\kappa_{10} = 0.59$; $\kappa_{11} = 0.59$; $\kappa_{12} = 0.52$; $\phi_9 = -0.02\pi$; $\phi_{10} = -0.20\pi$; $\phi_{11} = -0.40\pi$; $\phi_{12} = -0.58\pi$.
OSM	**MT (FSR 10 GHz):**	**OSBF (FSR 20 GHz):**
	$H_{\mathrm{MT}}(z)=\frac{\sqrt{1-\kappa_8}-e^{-j\phi_8}z^{-1}\sqrt{r}}{1-e^{-j\phi_8}z^{-1}\sqrt{r(1-\kappa_8)}}$	$H_{\mathrm{OSBF}}^{\mathrm{cross}}(z)=\frac{\sqrt{\kappa_{14}\kappa_{16}}(\sqrt{1-\kappa_{15}}-e^{-j\phi_{15}}rz^{-2})}{1-e^{-j\phi_{15}}rz^{-2}\sqrt{(1-\kappa_{15})}}+\frac{\sqrt{(1-\kappa_{14})(1-\kappa_{16})}(e^{-j\phi_{14}}\sqrt{r}z^{-1})}{1-e^{-j\phi_{15}}rz^{-2}\sqrt{(1-\kappa_{15})}}$
	$\kappa_8 = 0.87$; $\phi_8 = 0.50\pi$;	$\kappa_{14} = \kappa_{16} = 0.5$; $\kappa_{15} = 0.78$; $\phi_{14} = 0.20\pi$; $\phi_{15} = -0.40\pi$;
	κ_7 and κ_{13} to vary the inter-channel amplitude ratio; ϕ_7 and ϕ_{13} to synchronize the carrier phase.	

4. Experimental verification

To experimentally demonstrate the working of the proposed beamformer circuits, two sample circuits with the architectures shown in Fig. 3 were used, which are parts of a reconfigurable complex microwave photonic signal processor chip fabricated in a low-loss, high-index-contrast Si_3N_4/SiO_2 waveguide technology (TriPleX [23, 44]). The chip has multiple optical inputs and outputs, which allows us to get access to the circuits of question independently. To enable full operation, the chip has been fully packaged with electrical connections to all the tuning elements and fiber pigtails at both input and output sides, a photo of which is shown in Fig. 5(a). The setups to characterize the circuits and to verify the beamforming functionality are shown in Fig. 5(b) and 5(c), respectively. The circuit parameters (κ and ϕ) are configured via the on-chip thermo-optical tuning elements implemented using resister-based heaters [23, 44]. A scalable 12-bit voltage control system (from SATRAX B.V.) was used to drive multiple heaters simultaneously. The other major components in the setups include a 1.55 μm-wavelength single-frequency CW laser (Gooch & Housego, EM4-253-80-057) driven by a low-noise current controller (ILX Lightwave, LDX-3620), a Mach-Zehnder intensity modulator (Avanex, PowerLog FA-20), two phase modulators (EO space, PM-5K5-10), an RF detector (Discovery semiconductor, DSC-R401HG), and an RF vector network analyzer (Agilent, NA5230A PNA-L).

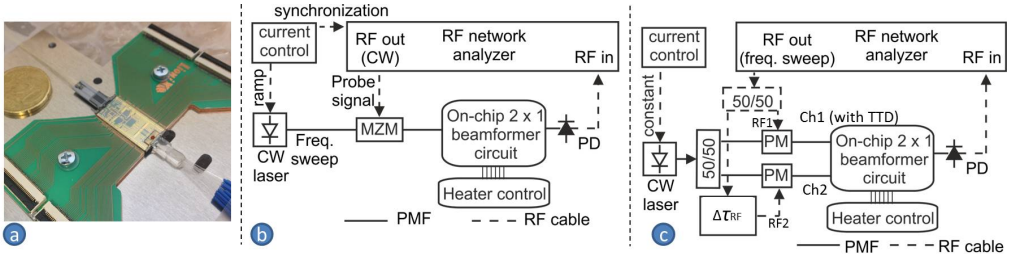

Fig. 5. (a) a photo of the fully packaged microwave photonic signal processor chip containing the beamformer circuits of question, (b) the measurement setup for the first step of setting the beamformer circuit parameters, (c) the setup to demonstrate in a second step the desired 2 × 1 beamforming functionality.

#211835 - $15.00 USD Received 9 May 2014; revised 26 Jun 2014; accepted 27 Jun 2014; published 3 Jul 2014

4.1 Beamformer circuit setting

As the first step, the setup in Fig. 5(b) is used to characterize the frequency responses of the beamformer circuits by means of the so-called phase-shift method [44]. Here, a probe-signal-modulated optical carrier is frequency-swept across a full free spectral range of the circuit under test, and the frequency response in the optical domain is acquired from the detected probe signal. In our case, a probe signal of 50 MHz generated by the RF network analyzer was chosen to achieve satisfying measurement resolution and accuracy simultaneously. The beamformer circuits were configured to match the calculated frequency responses as shown in Fig. 4. The measurements of the achieved frequency responses for the two circuits are presented in Fig. 6 and 7, respectively, where the calculated responses are also depicted showing an excellent agreement. As shown in Fig. 5(a) and 6(a), the TTDs of circuit 1 and 2 provide actual bandwidths of 16 GHz and 8 GHz, respectively, for the delay value of 0.3 ns (the beamformer channel without TTD is used as delay and loss reference). This satisfies the delay bandwidth requirements in order to perform signal synchronization between the two beamformer channels (delay bandwidth ≥ 14 GHz for circuit 1; ≥ 7 GHz for circuit 2). The additional loss due to the equivalent delay path length is seen to be about 1.2 dB, which is consistent with a waveguide propagation loss of 0.15 dB/cm. The reduced transmission of the TTD may cause an initial offset of the signal amplitude ratio between different beamformer channels. However, in practice this offset can be compensated at the tunable signal combiners (κ_7 and κ_{13} in Fig. 3), and therefore will not affect the beamforming functionality of the circuit. It can be seen in Fig. 6(b) and 7(b) that also the achieved MT and OSBF responses are in excellent agreement with the calculations. In addition, the transmission loss of the MT and the dispersion in the OSBF passband are also shown in the measurement results, which both have insignificant values in the frequency regions covering the optical signal and therefore should guarantee satisfying performances with negligible signal distortion.

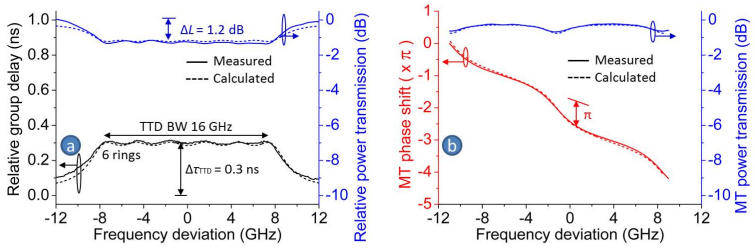

Fig. 6. Measured (solid) and calculated (dashed) frequency responses of circuit 1: (a) group delay and power transmission of the delay line (TTD) consisting of a cascade of 6 ring resonators, where the beamformer channel without TTD is regarded as delay and loss reference; (b) phase shift and power transmission of the modulation transformer (MT).

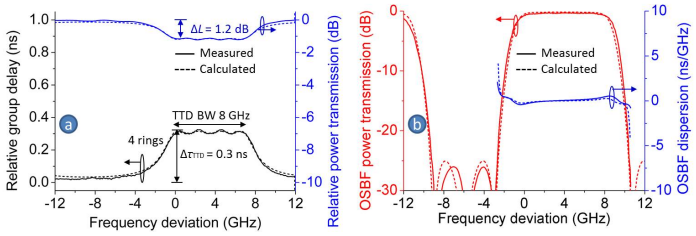

Fig. 7. Measured (solid) and calculated (dashed) frequency responses of circuit 2: (a) group delay and power transmission of the delay line (TTD) consisting of a cascade of 4 ring resonators, where the beamformer channel without TTD is regarded as the delay and loss reference; (b) power transmission of the optical sideband filter (OSBF) and the dispersion in the OSBF passband (the dispersion in the OSBF stopband is skipped for simplicity as it is not of relevance to the device functionality).

#211835 - $15.00 USD Received 9 May 2014; revised 26 Jun 2014; accepted 27 Jun 2014; published 3 Jul 2014

4.2 Demonstration of the beamformer system

With the circuit settings as described, the second step was demonstrating the desired beamforming functionality, for which we used the experimental setup in Fig. 5(c). An input RF signal sweeping from 10 MHz to 10 GHz is generated by the network analyzer and equally split to be employed as the driving signals for the two phase modulators in the beamformer system. In this setup, an RF delay $\Delta\tau_{RF}$ between the two driving signals is applied to simulate an according inter-antenna-element delay, while all other RF and optical connections for the two beamformer channels were made equal in length. First, the beamformer circuit 1 configured as in Fig. 6 is applied in the setup, and the optical carrier is tuned to the center of the group delay and power transmission spectrum (zero frequency in Fig. 6). Since this experimental setup uses several fiber connections between the laser and beamformer circuit chip instead of the desired full chip-level integration, special care was taken with mechanical and thermal stability in order to maintain the carrier phase relation between the beamformer channels.

With the setup ready, the RF-to-RF transmission of the two beamformer channels was first measured to verify the achievement of the desired system RF bandwidth of 4 GHz, namely the specified antenna reception band ranging from 3–7 GHz. For this measurement, only one RF drive was connected to its modulator at a time. The measurement results are depicted in Fig. 8(a). As explained earlier, the coupler κ_7 was adjusted such that the two beamformer channels have equal amplitude. The envelope profile of the measured RF-to-RF transmissions agrees with the theory regarding the bandpass property of the PM/DD scheme employing a ring resonator-based MT [46]. The RF transmission envelope of the beamformer channel with TTD (Ch1) has a good symmetric profile with respect to the center frequency of the RF passband, similar to that of the other channel without TTD (Ch2). This indicates that the optical carrier is positioned at the center of the delay band of TTD as desired, so that the two sidebands of the optical signal experience equal delays and losses and therefore avoid an additional RF fading at the detection as the effect of sideband imbalance.

Next, two RF drives, RF1 and RF2, were connected to the modulators simultaneously, and a RF delay $\Delta\tau_{RF} = 0.3$ ns was applied to RF2 to simulate the signal reception delay difference between the two antenna elements. In this case, $\Delta\tau_{RF} = \Delta\tau_{TTD}$, so that the two beamformer channels were delay-synchronized. After matching the optical carrier phases between the two beamformer channels, the 2 × 1 beamforming effect, namely an RF transmission gain of 6 dB, was achieved in agreement with theory [28]. This is depicted in Fig. 8(b). To further verify the correct operation of the beamformer circuit, an intentionally deviating delay was chosen between the two beamformer channels, $\Delta\tau_{diff} = \Delta\tau_{RF} - \Delta\tau_{TTD} = 0.67$ ns, which corresponds to microwave signals being incident on the antenna plane at a different angle than the beamformer is set for. Theoretically, this will result in frequency-periodic nullings in the RF transmission spectrum at the beamformer output [50], where the frequency period is determined by $\Delta f = 1/\Delta\tau_{diff} = 1.5$ GHz. A measurement on this was performed and exhibited agreement with the theory, the result of which is depicted in Fig. 8(c).

Likewise, the similar functionality of beamformer circuit 2 was also demonstrated, the results of which are depicted in Fig. 9. The measurement results in Fig. 8 and 9 prove the principles of the proposed MWP beamformer system operating with PM and DD, and verify the on-chip implementations of the proposed beamformer circuits.

#211835 - $15.00 USD Received 9 May 2014; revised 26 Jun 2014; accepted 27 Jun 2014; published 3 Jul 2014

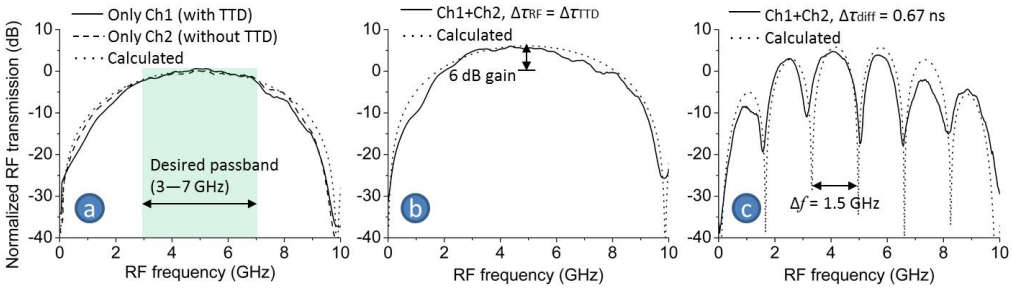

Fig. 8. Measured RF-to-RF transmissions of the demonstrator setup with beamformer circuit 1, normalized to the maximum transmission of Ch2: (a) only one RF drive is connected to its modulator at a time, which shows the system passband covers the desired 4 GHz bandwidth (3–7 GHz); (b) both RF drives are connected to the modulators and the two beamformer channels are delay-synchronized, which shows the 2 × 1 beamforming effect, namely a 6 dB gain in the passband; (c) an additional delay difference of 0.67 ns is introduced between the two beamformer channels, which causes periodic nullings with a frequency interval of 1.5 GHz as expected from theory.

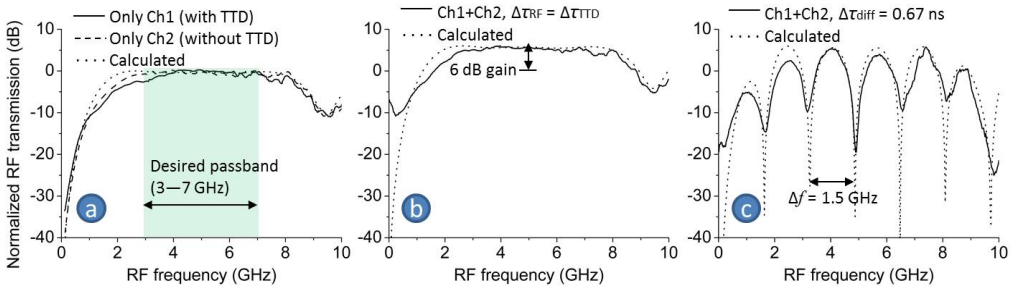

Fig. 9. Measured RF-to-RF transmissions of the demonstrator setup with beamformer circuit 2, normalized to the maximum transmission of Ch2: (a) only one RF drive is connected to its modulator at a time, which shows the system passband covers the desired 4 GHz bandwidth (3–7 GHz); (b) both RF drives are connected to the modulators and the two beamformer channels are delay-synchronized, which shows the 2 × 1 beamforming effect, namely a 6 dB gain in the passband; (c) an additional delay difference of 0.67 ns is introduced between the two beamformer channels, which causes periodic nullings with a frequency interval of 1.5 GHz as expected from theory.

5. Conclusions

In this paper, we have presented a novel microwave photonic beamformer system which operates with phase modulation and direct detection. The system can be constructed using two different on-chip beamformer circuit architectures. Both circuits consist of a beamforming network employing ring resonator-based delay lines and an optical sideband manipulator. The optical sideband manipulator can be implemented using a modulator transformer based on a ring resonator, or using an optical sideband filter based on a resonator-assisted Mach-Zehnder interferometer structure. To verify the principles in an experimental demonstration, a beamformer demonstrator has been presented in the most basic case, a two-element phased array receive antenna with instantaneous frequency band from 3–7 GHz, which exhibits the expected 2 × 1 beamforming functionality. The demonstration clearly shows the 6 dB signal enhancement for delay-synchronized reception and frequency-selective signal suppression for delay-deviated reception, which agrees well with the theory. The proposed MWP beamformer features simple device complexity, robustness, and scalability. In addition to this, its constitution promises a low-risk realization of fully integrated MWP beamformer systems, which is the key feature for system cost reduction in future development.

#211835 - $15.00 USD Received 9 May 2014; revised 26 Jun 2014; accepted 27 Jun 2014; published 3 Jul 2014

Acknowledgment

The research work presented in this paper was partially financed by Agentschap NL, the Netherlands, under an IOP project with no. IPD12009 (Promise2Day) and a Dutch Point One R&D Innovation project with no. PNE101008 (SATRAX), and partially funded by the European Community's Seventh Framework Program (FP7/2007-2013) under Grant Agreement no. 233679 (SANDRA). The authors are thankful to the finance providers for enabling this research.

#211835 - $15.00 USD Received 9 May 2014; revised 26 Jun 2014; accepted 27 Jun 2014; published 3 Jul 2014